EXPLORATION OF EARTH'S MAGNETIC FIELD BY HIGH ALTITUDE BALLOONS

6 authors, including:

Arie Sheinker
Soreq Nuclear Research Center
21 PUBLICATIONS   **646** CITATIONS

SEE PROFILE

Boris Ginzburg
Soreq Nuclear Research Center
26 PUBLICATIONS   **756** CITATIONS

SEE PROFILE

Joseph Ashkenazy
Soreq Nuclear Research Center
76 PUBLICATIONS   **863** CITATIONS

SEE PROFILE

EXPLORATION OF EARTH'S MAGNETIC FIELD BY HIGH ALTITUDE BALLOONS

Asaf Yaniv, Arie Sheinker, Boris Ginzburg, Nizan Salomonski, Joseph Ashkenazy, and Kobi Kutsher

Soreq Nuclear Research Center, Yavne 81800, Israel, Email: asafya@soreq.gov.il

ABSTRACT

Global Earth's magnetic field models widely used in physics of the Earth, magnetic mapping and directional drilling are mainly based on magnetic measurements at ground level, low altitudes and at space, whereas high altitudes magnetic data is scarce. In this work, we have tested advanced Earth's magnetic field models accuracy at altitudes reaching 28 km using a high altitude balloon carrying a magnetometer. A three-axis fluxgate magnetometer (FGM) was calibrated using an enhanced model, which enables accurate measurements within a wide temperature range. The measured magnetic field was compared to several Earth's magnetic field models, best coinciding with the enhanced magnetic model (EMM2017), with mean error of 12 nT and standard deviation of 19 nT, at altitudes above 5 km.

1. INTRODUCTION

The three main sources of the Earth's magnetic field are the core field, the crust field, and the disturbance field. The strongest contribution by far is the core field originating in the liquid iron flowing in the Earth's outer core. The disturbance field is produced by electric currents flowing in the upper atmosphere and near Earth space mainly originated by the sun activity [1].

Traditional Earth's magnetic field models such as the International Geomagnetic Reference Field (IGRF) and the World Magnetic Model (WMM) mainly account for the core field [2]. They use spherical harmonics analysis, where the model parameters are calculated using measurements obtained by magnetic observatories and satellites. Advanced models such as the Enhanced Magnetic Model (EMM) also account for the crust field [3]. Much higher resolution is allowed by incorporating magnetic data obtained by field surveys.

Since most of the data for calculating model parameters is obtained at low altitudes and space, magnetic data at high altitudes is scarce, and therefore the model accuracy at high altitudes is not yet been fully studied.

In order to investigate the Earth's magnetic field at high altitudes we proposed and implemented a balloon for measurements. A high altitude balloon carrying a payload including a GPS receiver and a magnetometer, enables the mapping of the Earth's magnetic field along its track at relevant altitudes.

2. PAYLOAD DEVELOPMENT

Since chances for retrieving the payload after landing are weak, e.g., the payload may fall into the Mediterranean Sea, we followed two guidelines in the design of the payload. First, using off-the-shelf components reduces the cost of a one-time payload. Second, transmitting the measured data back to a ground station, rather than storing it in real-time and retrieving it later on after the payload is found. These guidelines led us to choose the M10s radiosonde produced by Meteomodem (Fig.1).

Figure 1. M10s radiosonde produced by Meteomodem including a GPS receiver, RF transmitter, temperature and humidity sensors and an auxiliary input which was used to hook up the magnetometer

The M10s, originally intended for meteorological measurements, includes a GPS receiver, temperature and humidity sensors, and a radio transmitter with an auxiliary digital input. Thus, in addition to transmitting its location and meteorological data, the M10s enables to transmit additional data, such as magnetic measurements. In order to take magnetic measurements we have used the APS1540 (Applied Physics Systems, Fig.2). The APS1540, is a tri-axis FluxGate Magnetometer (FGM) with dynamic range of ±65,000 nT and a noise level of less than 0.5 nT. This FGM requires a unipolar power supply of +4.95 to +9 V while its current consumption is less than 55 mA. An internal 24-bit analog-to-digital converter provides a digital serial output with data rates of 10 readings per second in the ASCII mode or 20 readings/sec in the binary mode.

Figure 2. The APS1540 tri-axial fluxgate magnetometer

The magnetometer was serially connected to a beaglebone black (BBB) prototype board, which was programmed to read the magnetometer data and transfer it to the M10s transmitter using a suitable protocol.

The payload case was made from Polyethylene foam, which is light, heat-insulating, and non-magnetic. One meter separation between magnetometer and electronics guaranties low level of magnetic interference (Fig. 3).
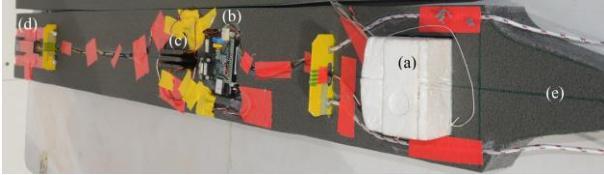

Figure 3. The payload includes (a) M10S radiosonde, (b) Beaglebone black with a voltage distribution module, (c) Lithium battery pack, and (d) APS1540s tri-axial magnetometer. The case (e) is made from Polyethylene foam

In order to mitigate magnetic interference, we replaced the batteries of the M10s and its antenna, with compatible non-magnetic parts.

Vector magnetometers suffer from imperfections such as non-orthogonal axes, offsets, non-linearity and susceptibility to temperature variations [4]. The aforementioned imperfections result in increasing measurement errors for a moving platform.

Therefore, total-field magnetometers are naturally a more suitable choice for moving platforms than vector magnetometers [5]. However, the larger weight, the higher current consumption, and the higher price of total-field magnetometers, forced us to choose a vector magnetometer for the payload. The usage of a suspension is only effective for the vertical axis [6]. In order to overcome the above imperfections, and to compensate for the payloads magnetic interference, we have calibrated the tri-axial magnetometer. First, we adopted a model for the magnetometer including transfer coefficients, axes mis-orthogonality, and offsets. Second, we rotated the magnetometer around each axis and recorded its output. In addition, we recorded simultaneously the output of a total-field magnetometer, which was used as a reference. The total-field magnetometer deployed in the vicinity of the tri-axial magnetometer is expected to sense the same Earth magnetic field as sensed by the tri-axial

magnetometer since the local gradient in our non-urban calibration area is extremely low. Third, the previous step was repeated for temperatures in the range of -25°c to +38°C, where the temperature was measured by the internal temperature sensor of the APS1540S magnetometer. Fourth, we applied curve fitting techniques to calculate each coefficient of the model as a function of the temperature. Hence, for every temperature value a set of different calculated coefficients was used to correct the tri-axial magnetometer. In order to finally check calibration results, the magnetometer was deployed in our magnetically 'clean' area for about 4 hours. Fig. 4 depicts the measured magnetic field before and after calibration. Fig. 5 depicts the temperature measured by the magnetometer internal sensor, which reflects the environmental temperature in addition to the magnetometer electronics heating. Notice that the magnetic field curve before calibration resembles the temperature change in Fig. 5. However, calibration cancels the temperature dependence as shown in Fig. 4.
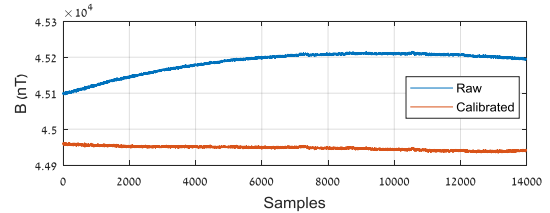

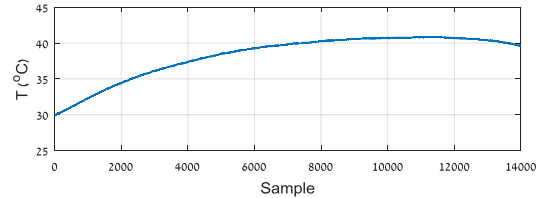*Figure 4. The measured magnetic field in our magnetically 'clean' area before and after calibration*

Figure 5. The temperature measured by the temperature sensor inside the magnetometer while measuring the magnetic field in our magnetically 'clean' lab

3. THE EXPERIMENT

A dedicated radio receiver from Meteomodem was used to receive the balloon's data. We have used a 6 m mast to enable good reception even at a large distance. A PC was employed to monitor the balloon progress and store the downlink data: GPS, temperature, and magnetic field readings. We also developed a software application to decode the magnetometer readings and present it in real-time.

We chose the HY-2000 balloon from Hwoyee for the flight. This high altitude balloon weighs 2 kg and nominally can reach altitudes of up to 38 km. Its neck is

14 cm in length and 7.9 cm in diameter. A flow meter was used to fill the balloon with 4.5 m^3 of helium. Calculations show that this amount of helium required for the balloon to climb at a velocity around 4-5 m/s and burst at altitude of around 34 km. Filling the balloon with more helium would result in faster climbing. However, the pressure inside the balloon would cause bursting at lower altitudes. On the other hand, filling the balloon with less helium would result in slower climbing which may result in crushing into trees and buildings before gaining enough height. In addition, when climbing too slowly the balloon may drift far and loose communication before reaching maximal altitude. The balloon was connected to the payload through a 1 m diameter parachute, which was intended to slow down the payload after the balloon bursting.
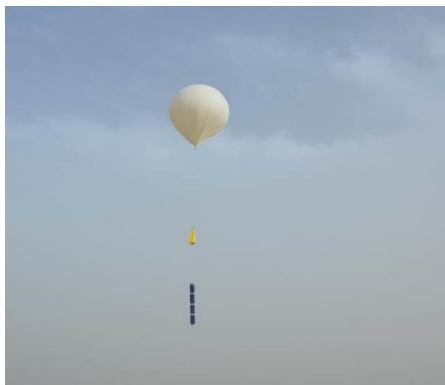
Figure 6. The balloon a few seconds after take-off

The balloon a few seconds after take-off is shown in Fig. 6. The balloon travelled for 3 hours, reaching an altitude of over 28 km, and distance of 350 km before communication was finally lost. Altitude and range of the payload are presented in Fig. 7 and Fig. 8 respectively.
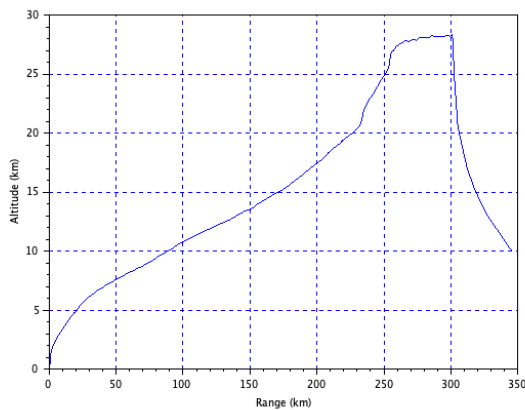

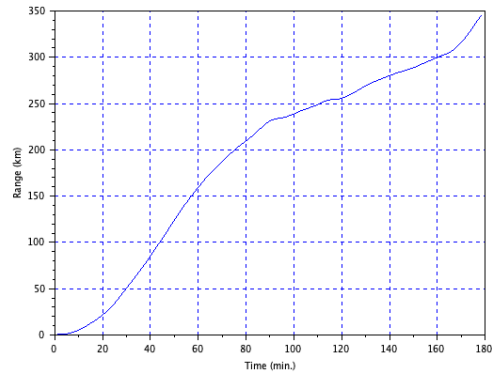*Figure 7. Balloon's altitude as a function of distance*

Figure 8. Balloon's distance as a function of time

The flight can be divided into three main phases which are summarized in Tab. 1 bellow. We assume that a small leak, developed during flight, might be the cause of the hovering phase, while at the same time prevented the balloon from reaching higher altitude.

Table 1. Flight's three main phases

	Distance	Time	Remarks
Ascending	260 km	120 min.	
Hovering	40 km	40 min.	Alt. ~ 28 km
Descending	50 km	20 min.	After bursting

Communication loss at distance of 350 km at altitude of 10 km is expected when the line-of-sight is blocked due to Earth's curvature. Fig. 9 depicts the no-communication periods along the flight, where at the distance of around 300 km the no-communication periods become significantly longer.
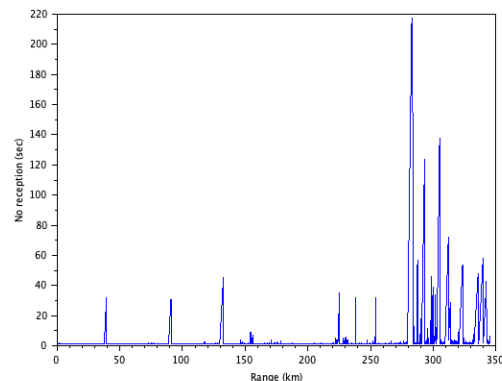

Figure 9. Communication loss periods as a function of distance

As mentioned above, two separated temperature sensors were included in the payload. The temperature sensor embedded in the M10s radiosonde, was physically near the wall of the Polyethylene case and therefore measured much cooler temperatures than the APS1540S

internal temperature sensor. The temperatures measured during the flight are depicted in Fig. 10.
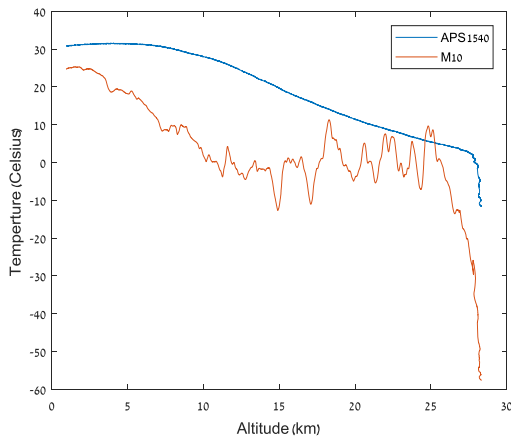

Figure 10. Temperatures measured during the flight

4. EXPERIMENTAL RESULTS

A total-field magnetometer was used as a reference in order to monitor the Earth's magnetic field during the flight. Fig. 11 depicts the total-field magnetometer readings. Although, no irregular events, such as sun storms, were recorded, the 'disturbance' magnetic field in the take-off site changes by almost 10 nT during the flight time.

Figs. 12 – 14 depict the components of the magnetic field measured during the flight.

Fig. 15 depicts the measured magnetic field before and after calibration.

Figs. 16 - 18 depict the measured magnetic field and the magnetic field calculated using the Earth magnetic field models as a function of time, distance and altitude, respectively.
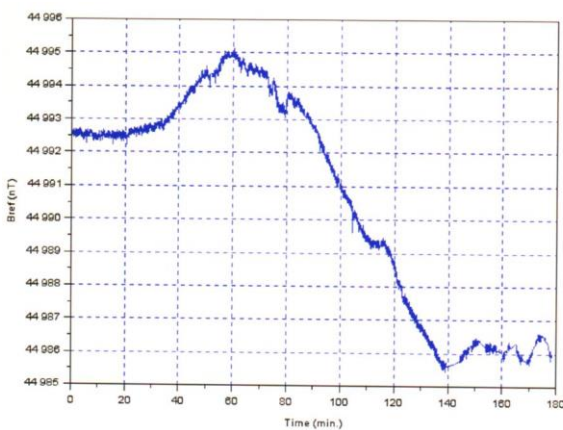

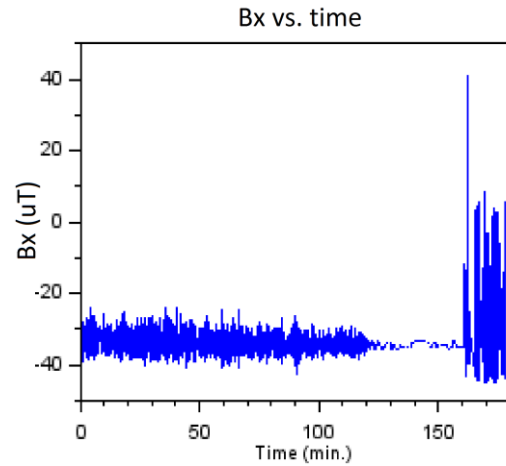Figure 11. The readings of the total field magnetometer used as a reference

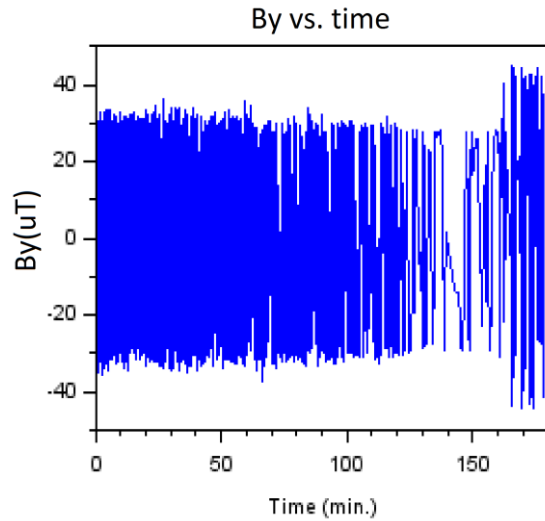Figure 12. Measured magnetic field along the x – $axis$ pointing in the vertical direction

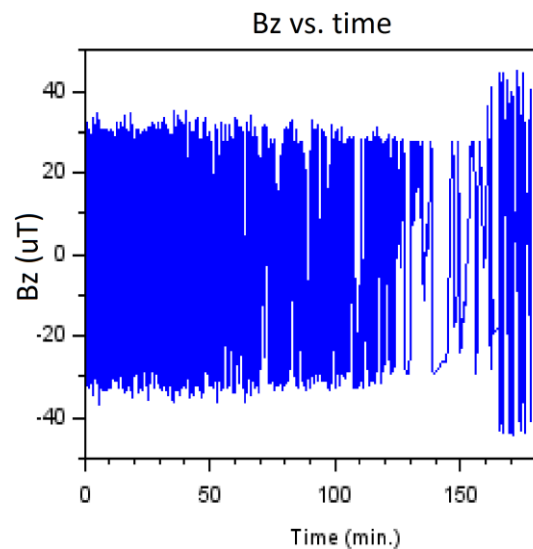

Figure 13. Measured magnetic field along the y – $axis$
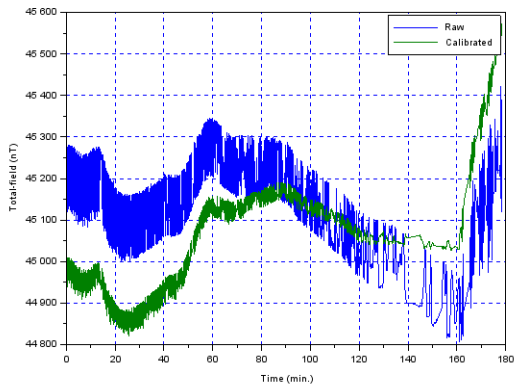

Figure 14. Measured magnetic field along the z – $axis$

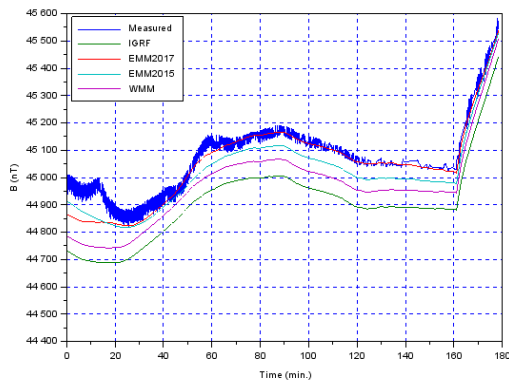*Figure 15. Measured magnetic field before and after calibration*

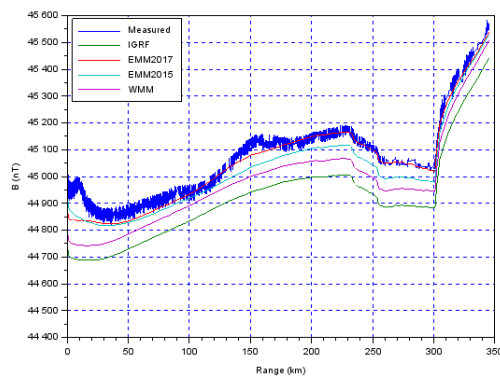*Figure 16. The magnetic field as a function of time*

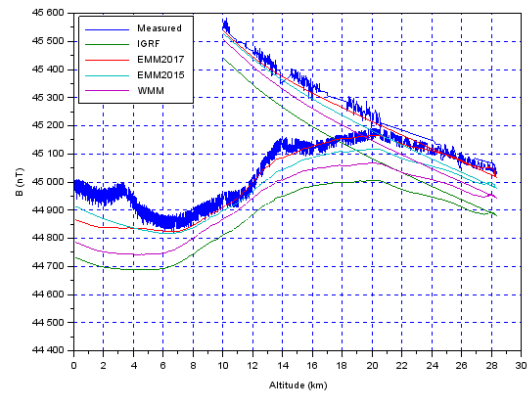*Figure 17. The magnetic field as a function of distance*

Figure 18. The magnetic field as a function of altitude

The errors between the measured magnetic field and the Earth's magnetic field models are display in Fig. 19. Notice from Fig. 18 that for altitudes above, say 5 km, the error becomes smaller than at lower altitude. This is because Earth's magnetic field models are more accurate at higher altitudes, where anomalies due to Earth's crust are negligible. Tab. 2 summarizes the overall errors, and the errors for altitudes above 5 km.
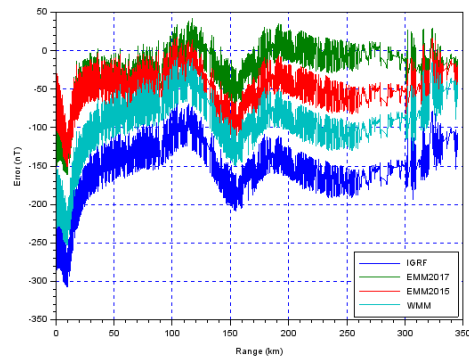

Figure 19. The error between the measured magnetic field and the Earth' magnetic field models

Table 2. Magnetic field errors

Model	Overall error (nT)		Error above 5 km (nT)	
	Mean	STD	Mean	STD
IGRF	-166	40	-154	23
WMM2015	-107	41	-94	22
EMM2015	-56	22	-51	18
EMM2017	-24	38	-12	19

5. DISCUSSION

As expected, among the Earth's magnetic field models the EMM2017 model, which is the most advanced and updated, shows the higher coincidence with the measured magnetic field. The mean error is -24 nT,

whereas the standard deviation (STD) is 38 nT. In case we consider altitudes above 5 km, the mean error reduces to -12 nT with STD of 19 nT, only.

The errors between the measured magnetic field and the EMM2015 model are slightly larger than for the EMM2017 model. The WMM2015 model is next, and finally the IGRF model, which is the model with the largest error relative to the measurements. For all the above models, the error decreases for higher altitudes. This can be explained by the fact that the models do not fully take into account local anomalies. These anomalies are mainly due to magnetic minerals in the crust and upper mantle.

There are measurement error sources which should be taken into account. The magnetometer noise consists of its intrinsic noise and noise caused by aforementioned imperfections. The calibration process mitigates the later noise and also compensates for platform interference, i.e., remnant and induced magnetization. Nevertheless, residual noise is still left.

Discrepancy between the measurements and the models may be due to GPS inaccuracies which also contribute to summary error.

The natural changes in Earth magnetic field is also an important factor. The reference magnetometer did not show extreme 'disturbance' field activity during the flight. However, the measured swing is about 10 nT at the take-off site, and may be even larger along the balloon trajectory.

6. CONCLUSION AND FURTHER WORK

We developed a payload for measuring the Earth's magnetic field consisting of an APS1540 tri-axial fluxgate magnetometer, and the M10s radiosonde including a GPS receiver, temperature sensor and a radio transmitter.

The payload was attached to a high-altitude HY-2000 balloon. The balloon was filled with 4.5 m^3 of helium and travelled for 3 hours. It reached an altitude of over 28 km and distance of about 350 km, before communication was lost.

The measured magnetic field was compared to existing Earth's magnetic field models: IGRF, WMM2015, EMM 2015, and EMM2017. The smallest error was obtained for the EMM2017 model which is the most advanced and updated model.

For altitudes above 5 km the error between the measured magnetic field and the models is smaller than for lower altitudes, which suggests that the model do not fully account for local anomalies due to magnetic minerals in the crust and upper mantle.

We plan to carry out additional balloon experiments in order to explore the Earth's magnetic field and its models at various locations.

8. REFERENCES

1. Wallace H. Campbell. *Introduction to Geomagnetic Fields (2003, 2nd edition)*, Cambridge University

2. Chulliat, A., S. Macmillan, P. Alken, C. Beggan, M. Nair, B. Hamilton, A. Woods, V. Ridley, S. Maus and A. Thomson (2015) , The US/UK World Magnetic Model for 2015-2020: *Technical Report, National Geophysical Data Center*, NOAA.

3. Chulliat, A., P. Aiken, M. Nair, A. Woods, and S. Maus (2015), The Enhanced Magnetic Model 2015-2020, *National Centers for Environmental Information*, NOAA.

4. Merayo J. M. G., Brauer P., Primdahl F., Peterson J. R. and Nielsen O. V. (2000). Scalar Calibration of Vector Magnetometers, *Measurements Science and Technology*, 11, pp. 120-132.

5. A. PRYSTAI, V. KOREPANOV, F. DUDKIN and B. LADANIVSKYY (2016). Vector Magnetometer Application with Moving Carriers. *Sensors & Transducers, Vol. 207, Issue 121*.

6. V. KOREPANOV, F. DUDKIN and Y. Tsvetkov (2005). GRADIENT MAGNETOMETER SYSTEM FOR BALLOONS. *ESA SP-590.*